Data report: rate- and state-dependent friction parameters of core samples from Site C0019, IODP Expedition 343 (JFAST)[1]

Matt J. Ikari[2]

Chapter contents

[1]Ikari, M.J., 2015. Data report: rate- and state-dependent friction parameters of core samples from Site C0019, IODP Expedition 343 (JFAST). *In* Chester, F.M., Mori, J., Eguchi, N., Toczko, S., and the Expedition 343/343T Scientists, *Proc. IODP,* 343/343T: Tokyo (Integrated Ocean Drilling Program Management International, Inc.). doi:10.2204/iodp.proc.343343T.203.2015
[2]MARUM, Center for Marine Environmental Sciences, University of Bremen, D-28359 Bremen, Germany. mikari@marum.de

Abstract

This report explains shearing tests conducted on samples collected throughout the main cored interval at Site C0019 during Integrated Ocean Drilling Program Expedition 343, the Japan Trench Fast Drilling Project. This site is located within the region of high coseismic slip during the 2011 Tohoku earthquake that reached the ocean floor at the Japan Trench. Results of velocity-stepping tests within 0.1–30 µm/s on both intact and powdered samples allowed quantification of the rate- and state-dependent friction constitutive parameters a-b, a, b_1, b_2, D_{c1} and D_{c2} by inverse modeling techniques. Also reported here are measurements of the initial friction prior to each step (μ_o) and the slip-dependence of friction (η), which were used as input parameters to the model. Downhole patterns of friction parameters are observed to correlate consistently with lithology. For powdered samples, the fault zone, a siliceous mudstone ~2 m below the fault zone, and three pelagic clay samples can be distinguished from hanging wall and underthrust footwall siliceous mudstones by lower a, lower b, higher a-b. These results indicate a tendency for velocity strengthening, lower friction, and higher η,which indicates a tendency for slip-hardening. Intact samples show the same patterns, albeit with fewer data points. Aside from the lithologic control, strong downhole trends in the friction parameters are not observed.

Introduction

The slip behavior of major fault zones, especially at shallow depths, is controlled by the frictional behavior of the active shear zone. The 2011 Mw 9.0 Tohoku earthquake produced largely unexpected 30–80 m of shallow coseismic slip that breached the Japan Trench (Fujiwara et al., 2011; Ide et al., 2011; Ito et al., 2011). That the shallowest reaches of the Japan Trench in the Tohoku area facilitated such a large amount of coseismic slip propagation is inconsistent with current understanding of fault mechanics, and explaining this phenomenon therefore requires thorough characterization of megathrust fault zone frictional properties in this region (e.g., Lay and Kanamori, 2011). Drilling during Integrated Ocean Drilling Program (IODP) Expedition 343, the Japan Trench Fast Drilling Project (JFAST) penetrated the toe of the prism at the Japan Trench subduction zone ~5 km landward of the trench axis, within the area of high coseismic slip and directly

updip from the Tohoku earthquake hypocenter (Fig. F1). Successful recovery of core samples of the fault zone that hosted the 2011 Tohoku earthquake, as well as the surrounding wall rocks, in the ~840 m deep borehole has provided the opportunity to investigate the frictional properties of the shallow plate boundary megathrust in the Tohoku.

Sample descriptions

The sample suite in this study consists of 21 samples recovered by rotary barrel coring between 648 and 837 meters below seafloor (mbsf) (Table T1). Seventeen of these samples are siliceous mudstones that make up the hanging wall prism and underthrust footwall (lithologic Units 2, 3, and 5) and are relatively structureless (see the "Site C0019" chapter [Expedition 343/343T Scientists, 2013b]). The remaining samples include one sample from a highly sheared scaly clay layer (Unit 4) interpreted to be the plate boundary fault zone at 821.5–822.5 mbsf (Chester et al., 2013), and three samples of a multicolored, stratified pelagic clay layer located ~10 m below the fault zone (Unit 6). Unlike the fault zone, the pelagic clay exhibits no shear fabric (see the "Site C0019" chapter [Expedition 343/343T Scientists, 2013b]). Seven of the samples were recovered in a sufficient condition to be tested intact: four hanging wall mudstones, one from the fault zone, and one footwall mudstone. The final intact sample was recovered in Core 343-C0019E-21R from the bottom of the borehole; however, this sample is a mudstone rather than the chert that defines Unit 7, and therefore is probably a Unit 3 sample that fell into the borehole. All 21 samples were tested as gouge powders; therefore, the seven intact samples can be directly compared with a powdered sample of equivalent composition.

Rate- and state-dependent friction

Many studies over the years have demonstrated with laboratory shearing experiments that fault strength is dependent on the sliding velocity (see Marone, 1998, and references therein). In such experiments, the coefficient of sliding friction μ is calculated from the measured shear strength:

$$\mu = \frac{\tau}{\sigma_n'}. \quad (1)$$

The velocity dependence of friction is then evaluated by instantaneously increasing (or sometimes decreasing) the sliding velocity from an initial value v_0 to a new value v in a stepwise fashion. The frictional response to an imposed velocity step is described by an empirically derived constitutive friction law (Dieterich, 1979, 1981):

$$\mu = \mu_0 + a\ln\left(\frac{v}{v_0}\right) + b_1\ln\left(\frac{v_0\theta_1}{D_{c1}}\right) + b_2\ln\left(\frac{v_0\theta_2}{D_{c2}}\right), \quad (2)$$

$$\frac{d\theta_i}{dt} = 1 - \frac{v\theta_i}{D_{ci}}, i = 1, 2, \quad (3)$$

where a, b_1, and b_2 are unitless constants and D_{c1} and D_{c2} are critical slip distances, over which friction evolves over durations measured as θ_1 and θ_2, the state variables (Fig. F2). Because the frictional response depends on both the velocity v and the state variable θ, this formulation is known as rate- and state-dependent friction (RSF).

If the friction level at the higher velocity v has reached steady-state, Equations 2 and 3 can be reduced to:

$$a\text{-}b = \frac{\Delta\mu_{ss}}{\Delta\ln v}, \quad (4)$$

where the parameter a-b quantifies the rate-dependence of friction. This is the most important and widely used parameter because it controls the occurrence of slip instability that results in earthquake nucleation (e.g., Scholz, 1998). If a-b > 0, known as velocity-strengthening friction, slip is expected to be stable. On the other hand, a-b < 0 defines velocity-weakening behavior, which is a necessary condition for unstable slip. The RSF parameters, including a-b, have been used in numerical modeling studies to successfully simulate and describe a wide range of fault-slip phenomena, including earthquake nucleation and rupture (e.g., Okubo, 1989; Dieterich, 1992), afterslip (e.g., Perfettini and Avouac, 2007), and transient slow slip events (e.g., Liu and Rice, 2009).

Experimental methods

Laboratory friction experiments were performed by shearing the samples in a single direct shear device (see Ikari and Kopf, 2011) (Fig. F3). In this apparatus, the sample volume is a vertically oriented cylinder 25 mm in diameter and with a height of ~12–20 mm within a cell consisting of two flat-lying steel plates. Intact samples were carved from whole-round cores to fit exactly into the sample cell. Powdered samples were prepared by drying the samples at room temperature, disaggregating by hand in a mortar and pestle, and sieving to a maximum grain size of 125 μm. The powders were then mixed with a small amount of 3.5% NaCl brine to form a paste, which was then pressed into the sample cell. Samples were then loaded to a target normal stress (σ_n) of ~5–7 MPa to match in situ effective vertical stresses estimated from shipboard measurements of bulk density

(minus seawater density) and assuming hydrostatic fluid pressure conditions (see the **"Expedition 343/343T summary"** and **"Site C0019"** chapters [Expedition 343/343T Scientists, 2013a, 2013b]) (Table **T1**). Although the pore pressure cannot be directly controlled in this system, samples were allowed to consolidate overnight after application of normal load and allowed to freely drain through porous metal frits at the top and bottom of the sample. Shearing was only initiated after the sample height reached a steady value, indicating that any excess pore pressure had dissipated and the applied normal stress (σ_n) is equal to the effective normal stress (σ_n'). Shear is induced by relative displacement of the plates normal to the cylinder axis; for intact samples this means that the shear plane is not necessarily aligned with sample fabric, and this difference depends on the fabric dip. Deformation is in the apparatus is planar and therefore enforced to be localized. All tests were conducted under fluid-saturated conditions with 3.5% NaCl brine as the pore fluid. To ensure saturation during the tests, the sample cell is submerged in a pore fluid reservoir.

The experimental procedure involves shearing at a constant rate of 10 µm/s to a displacement of ~5 mm, in order to reach an approximate steady-state shear strength in which low-displacement effects (e.g., from fracturing near the peak strength) are minimized. In order to measure the velocity (or rate) dependence of friction, the shearing velocity was then increased in a series of steps within the range 0.1–30 µm/s (Fig. **F3**). The upstep velocity is $v = \sim 3v_0$, where v_0 is the initial velocity of each step. Although the parameter *a-b* may be calculated by directly measuring the steady-state friction change from a velocity step (Equation **4**), the individual RSF parameters a, b_1, b_2, D_{c1}, and D_{c2} must be calculated with modeling techniques due to covariance. An expression for the system stiffness k (friction/displacement) is incorporated:

$$\frac{d\mu}{dt} = k(v_{lp} - v), \qquad (5)$$

where $(v_{lp} - v)$ is the difference between true slip velocity v and the remotely recorded load point velocity v_{lp} due to apparatus deformation. The system stiffness includes the combined effects of apparatus and sample stiffness; for most testing equipment this is dominated by the apparatus stiffness. Equations **2**, **3**, and **5** are solved with a fifth-order Runge-Kutta numerical integration, and best-fit RSF parameters are obtained by solving the inverse problem with an iterative least-squares method (Fig. **F3**) (Reinen and Weeks, 1993). Due to variations in the experimental data caused by signal noise or excursions in the measurement, standard deviations for the modeled values are also calculated. In some cases, the data are well fit using one state variable, where $b_2 = 0$. Input parameters for the inversion include visual estimations of the RSF parameters, the initial friction level immediately preceding the velocity step μ_0, friction slip dependence $\eta = d\mu/dx$ at v (where x is slip displacement), and the system stiffness k (friction/displacement).

Results

Powdered samples

Values of a generally range between 0.003 to 0.009 for all samples except the fault zone sample from Section 343-C0019E-17R-1, the three pelagic clay samples from Section 20R-2, and the sample from Section 18R-1 from Unit 5 mudstones located ~2 m below the fault zone. These samples exhibited clearly lower values of $a < 0.004$ (Fig. **F4;** Table **T2**). Large scatter between –0.003 and 0.011 is observed for b_1 and b_2, with generally lower values occurring in the fault zone and pelagic clays. Instances of negative b are observed mostly in the white pelagic clay. For the critical slip distances, D_{c1} is typically less than ~15 µm and generally smaller than D_{c2}, which mostly clusters between ~40 and 200 µm. Larger values of D_{c1} ranging from ~20 µm up to several hundred micrometers are observed again for the fault zone, pelagic clay, and Section 18R-1 sample; however, in these cases the data were fit with one state variable, suggesting that the longer D_c is a typical value. Mostly velocity-weakening friction is observed throughout the borehole, with *a-b* approximately ranging between –0.01 and 0.005. Within the scatter, *a-b* appears to slightly increase from ~650 to 720 mbsf. The fault zone, pelagic clays, and 18R-1 sample tend to exhibit velocity-strengthening behavior (*a-b* up to ~0.004), but a few occurrences of velocity weakening are still observed in these samples. Initial friction values μ_0 are consistently between 0.43 and 0.58 and appear to slightly decrease from ~650 to 720 mbsf before becoming relatively constant downhole. Notably weak values of 0.18–0.29 are observed for the fault zone, Sample18R-1, and pelagic clay (Fig. **F4,** Table **T3**). The friction slip dependence parameter η shows a wide scatter between –0.025 and 0.01 mm^{-1}, but mostly negative values indicating slip-weakening friction. Again, exceptions include the fault zone, Sample 18R-1, and pelagic clay for which most of the slip-hardening is observed.

Intact samples

Due to the smaller number of samples, downhole trends are more difficult to identify for intact samples, but they exhibit many of the same characteristics as the powdered samples. No intact samples of the pelagic clay or Section 343-C0019E-18R-1 were tested, but one sample of the fault zone was tested in an intact state. For the intact wall rock mudstones (Units 3 and 5), a ranges from 0.003–0.007 but is <0.0024 in the fault zone (Fig. F5; Table T4). Both b_1 and b_2 range from 0.001 to 0.007; no negative values of b are observed. Values of b are clearly lower for the fault zone, ranging from 0.0004 to 0.0014. For mudstone samples, D_{c1} is usually less than ~15 µm, and values <10 µm are common, whereas D_{c2} values range from ~40 to 200 µm. Similar to observations from the powdered samples, the intact fault zone sample was well fit with one state variable; therefore, its D_c values of 35–90 µm match closely with the D_{c2} values of the mudstone wall rock. Velocity weakening is common for intact samples, with a-b as low as –0.008. The fault zone sample is velocity neutral to velocity strengthening (a-b = 0–0.002); however, some instances of velocity strengthening are also observed in the wall rock. The range of initial friction values for the mudstones is ~0.40–0.55, slightly lower than the range for powdered samples (Fig. F5; Table T5). Initial friction values for the fault zone cluster tightly at μ_0 = 0.21. Finally, the friction slip dependence ranges from –0.02 to 0.02 mm^{-1} and appears to increase with depth such that the fault zone and the mudstone below it (Section 343-C0019E-20R-1) exhibit only slip-hardening behavior, whereas the shallow samples exhibit slip weakening.

Acknowledgments

I thank Achim Kopf, Chris Marone, and André Niemeijer for helpful discussions and for providing access to the experimental apparatus and modeling software. Samples were provided by the Integrated Ocean Drilling Program (IODP) and collected during Expedition 343. This work was supported by the Deutsche Forschungsgemeinschaft Grant #IK107/1-1 to M.J.I.

References

Chester, F.M., Rowe, C., Ujiie, K., Kirkpatrick, J., Regalla, C., Remitti, F., Moore, J.C., Toy, V., Wolfson-Schwehr, M., Bose, S., Kameda, J., Mori, J.J., Brodsky, E.E., Eguchi, N., Toczko, S., and the Expedition 343 and 343T Scientists, 2013. Structure and composition of the plate-boundary slip zone for the 2011 Tohoku-oki Earthquake. *Science,* 342(6163):1208–1211. **doi:10.1126/science.1243719**

Dieterich, J.H., 1979. Modeling of rock friction: 1. Experimental results and constitutive equations. *J. Geophys. Res.: Solid Earth,* 84(B5):2161–2168. **doi:10.1029/JB084iB05p02161**

Dieterich, J.H., 1981. Constitutive properties of faults with simulated gouge. *In* Carter, N.L., Friedman, M., Logan, J.M., and Stearns, D.W. (Eds.), *Mechanical Behavior of Crustal Rocks: The Handin Volume.* Geophys. Monogr., 24:103–120. **http://onlinelibrary.wiley.com/doi/10.1029/GM024p0103/summary**

Dieterich, J.H., 1992. Earthquake nucleation on faults with rate- and state-dependent strength. *Tectonophysics,* 211(1–4):115–134. **doi:10.1016/0040-1951(92)90055-B**

Expedition 343/343T Scientists, 2013a. Expedition 343/343T summary. *In* Chester, F.M., Mori, J., Eguchi, N., Toczko, S., and the Expedition 343/343T Scientists, *Proc. IODP,* 343/343T: Tokyo (Integrated Ocean Drilling Program Management International, Inc.). **doi:10.2204/iodp.proc.343343T.101.2013**

Expedition 343/343T Scientists, 2013b. Site C0019. *In* Chester, F.M., Mori, J., Eguchi, N., Toczko, S., and the Expedition 343/343T Scientists, *Proc. IODP,* 343/343T: Tokyo (Integrated Ocean Drilling Program Management International, Inc.). **doi:10.2204/iodp.proc.343343T.103.2013**

Fujiwara, T., Kodaira, S., No, T., Kaiho, Y., Takahashi, N., and Kaneda, Y., 2011. The 2011 Tohoku-Oki earthquake: displacement reaching the trench axis. *Science,* 334(6060):1240. **doi:10.1126/science.1211554**

Ide, S., Baltay, A., and Beroza, G.C., 2011. Shallow dynamic overshoot and energetic deep rupture in the 2011 Mw 9.0 Tohoku-Oki earthquake. *Science,* 332(6036):1426–1429. **doi:10.1126/science.1207020**

Ikari, M.J., and Kopf, A.J., 2011. Cohesive strength of clay-rich sediment. *Geophys. Res. Lett.,* 38(16):L16309. **doi:10.1029/2011GL047918**

Ito, Y., Tsuji, T., Osada, Y., Kido, M., Inazu, D., Hayashi, Y., Tsushima, H., Hino, R., and Fujimoto, H., 2011. Frontal wedge deformation near the source region of the 2011 Tohoku-Oki earthquake. *Geophys. Res. Lett.,* 38(7):L00G05. **doi:10.1029/2011GL048355**

Lay, T., and Kanamori, H., 2011. Insights from the great 2011 Japan earthquake. *Phys. Today,* 64(12):33–39. **doi:10.1063/PT.3.1361**

Liu, Y., and Rice, J.R., 2009. Slow slip predictions based on granite and gabbro friction data compared to GPS measurements in northern Cascadia. *J. Geophys. Res.: Solid Earth,* 114(B09407). **doi:10.1029/2008JB006142**

Marone, C., 1998. Laboratory-derived friction laws and their application to seismic faulting. *Annu. Rev. Earth Planet. Sci.,* 26:643–696. **doi:10.1146/annurev.earth.26.1.643**

Okubo, P.G., 1989. Dynamic rupture modeling with laboratory-derived constitutive relations. *J. Geophys. Res.: Solid Earth,* 94(B9):12321–12335. **doi:10.1029/JB094iB09p12321**

Perfettini, H., and Avouac, J.-P., 2007. Modeling afterslip and aftershocks following the 1992 Landers earthquake. *J. Geophys. Res.: Solid Earth,* 112(B7):B07409. **doi:10.1029/2006JB004399**

Reinen, L.A., and Weeks, J.D., 1993. Determination of rock friction constitutive parameters using an iterative least squares inversion method. *J. Geophys. Res.: Solid Earth,* 98(B9):15937–15950. **doi:10.1029/93JB00780**

Scholz, C.H., 1998. Earthquakes and friction laws. *Nature,* 391(6662):37–42. **doi:10.1038/34097**

Initial receipt: 11 June 2014
Acceptance: 12 March 2015
Publication: 15 June 2015
MS 343343T-203

Figure F1. Map of the Tohoku area of the Japan Trench, showing the epicenter of the 2011 Tohoku earthquake, the location of Site C0019, and the location of seismic reflection Line HD33B. Lower panel is a cross-sectional profile of the toe of the Japan Trench prism, showing seismic reflection data from Line HD33B and the depth and location of the JFAST borehole, Hole C0019E. VE = vertical exaggeration. Modified from the **"Expedition 343/343T summary"** chapter (Expedition 343/343T Scientists, 2013a).

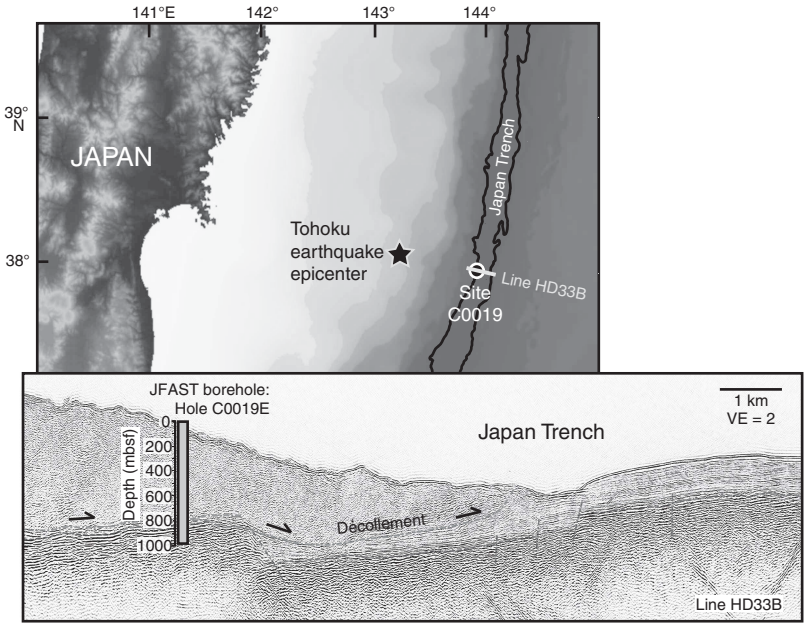

Figure F2. Schematic illustration of an idealized velocity step showing the role of individual rate- and state-dependent friction parameters. Friction slip dependence in this case is zero.

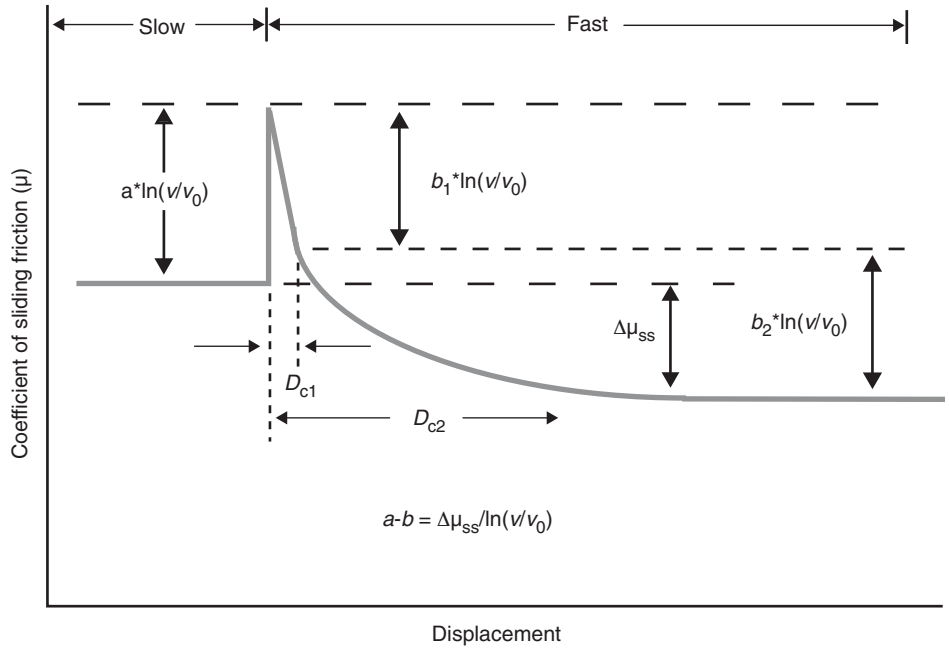

Figure F3. Example friction data for intact Sample 343-C0019E-12R-2. **A.** Complete friction-displacement curve showing where the velocity-stepping sequence was performed. Inset shows a schematic diagram of the single-direct-shear apparatus. **B.** Velocity-stepping sequence in A. **C.** Close-up view of the velocity step from 1 to 3 µm/s (box in B). Experimental data (gray) is overlain by data determined by inverse modeling (black).

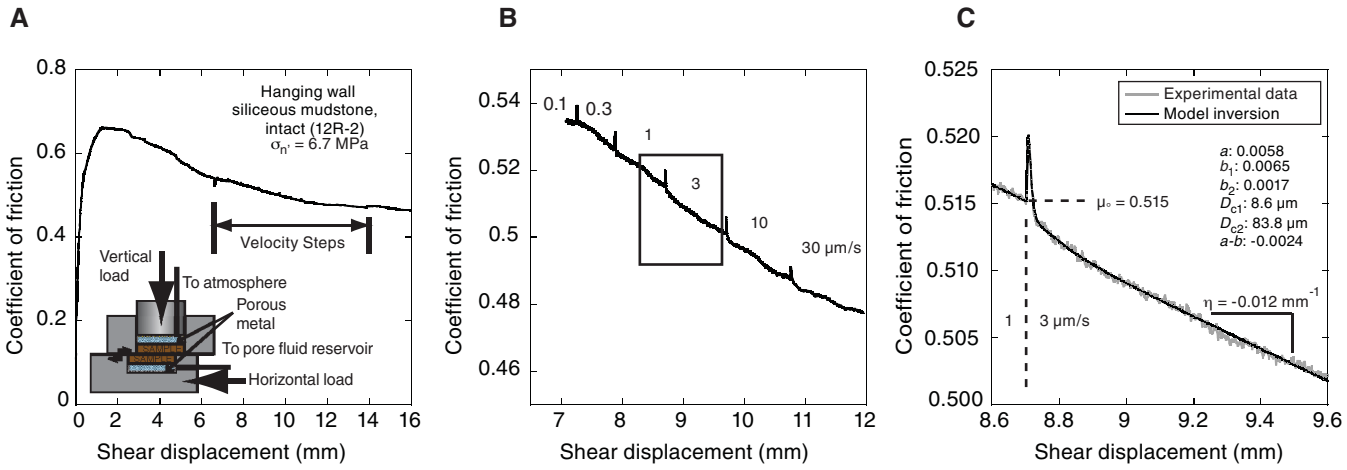

Figure F4. Rate- and state-dependent friction constitutive parameters (**A**) a, (**B**) b_1 and b_2, (**C**) D_{c1} and D_{c2}, (**D**) a-b obtained by inverse modeling, and the measured parameters (**E**) μ_0 and (**F**) η for powdered samples as a function of depth Hole C0019E. Downhole lithology shown for reference (see the "Site C0019" chapter [Expedition 343/343T Scientists, 2013b]). Red line indicates samples from the fault zone, purple line indicates samples from the pelagic clay layer.

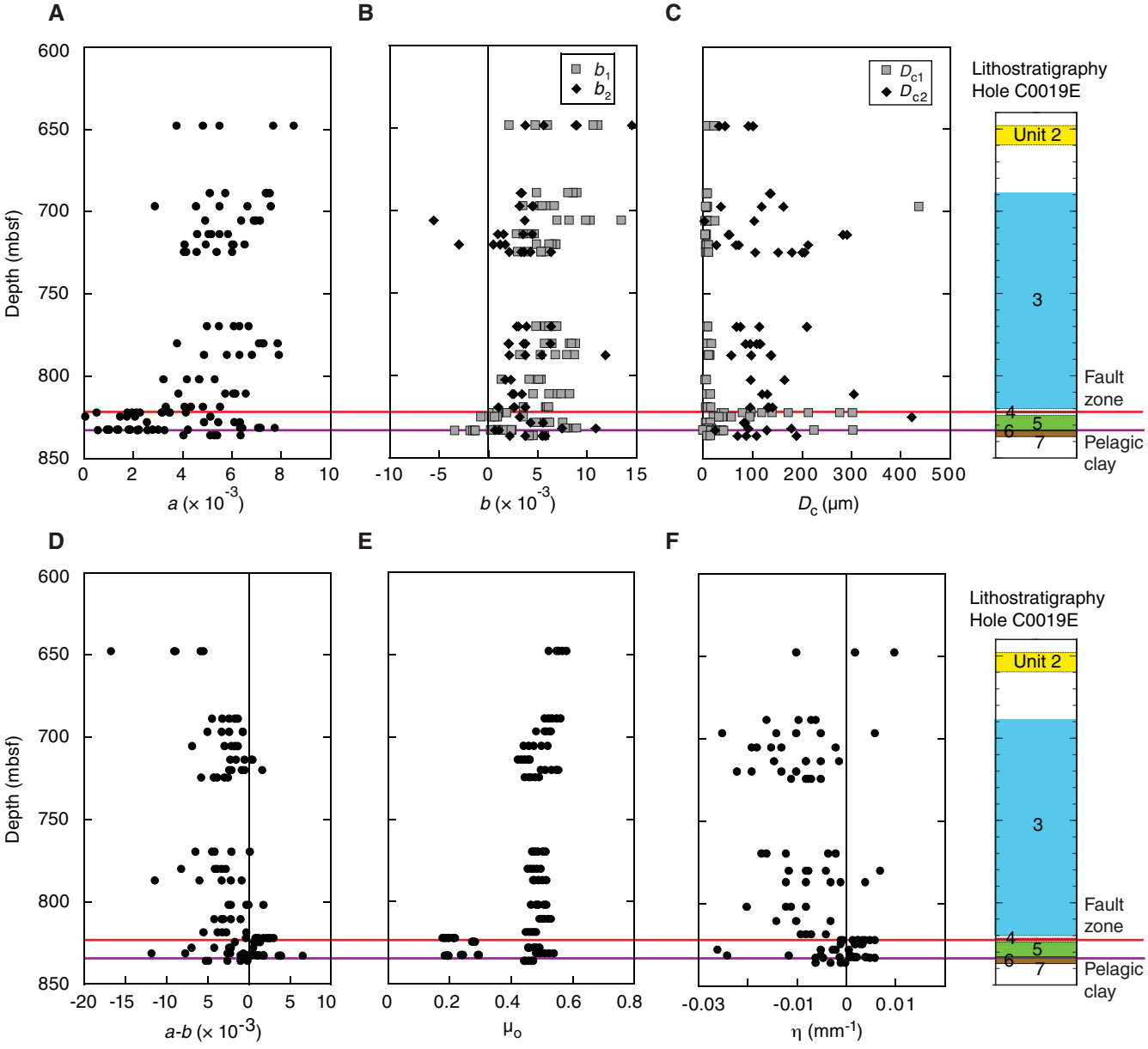

Figure F5. Rate- and state-dependent friction constitutive parameters (**A**) a, (**B**) b_1 and b_2, (**C**) D_{c1} and D_{c2}, (**D**) a-b obtained by inverse modeling, and the measured parameters (**E**) μ_0 and (**F**) η for intact samples as a function of depth in Hole C0019E. Downhole lithology shown for reference (see the "Site C0019" chapter [Expedition 343/343T Scientists, 2013b]). Red line indicates samples from the fault zone, purple line indicates samples from the pelagic clay layer.

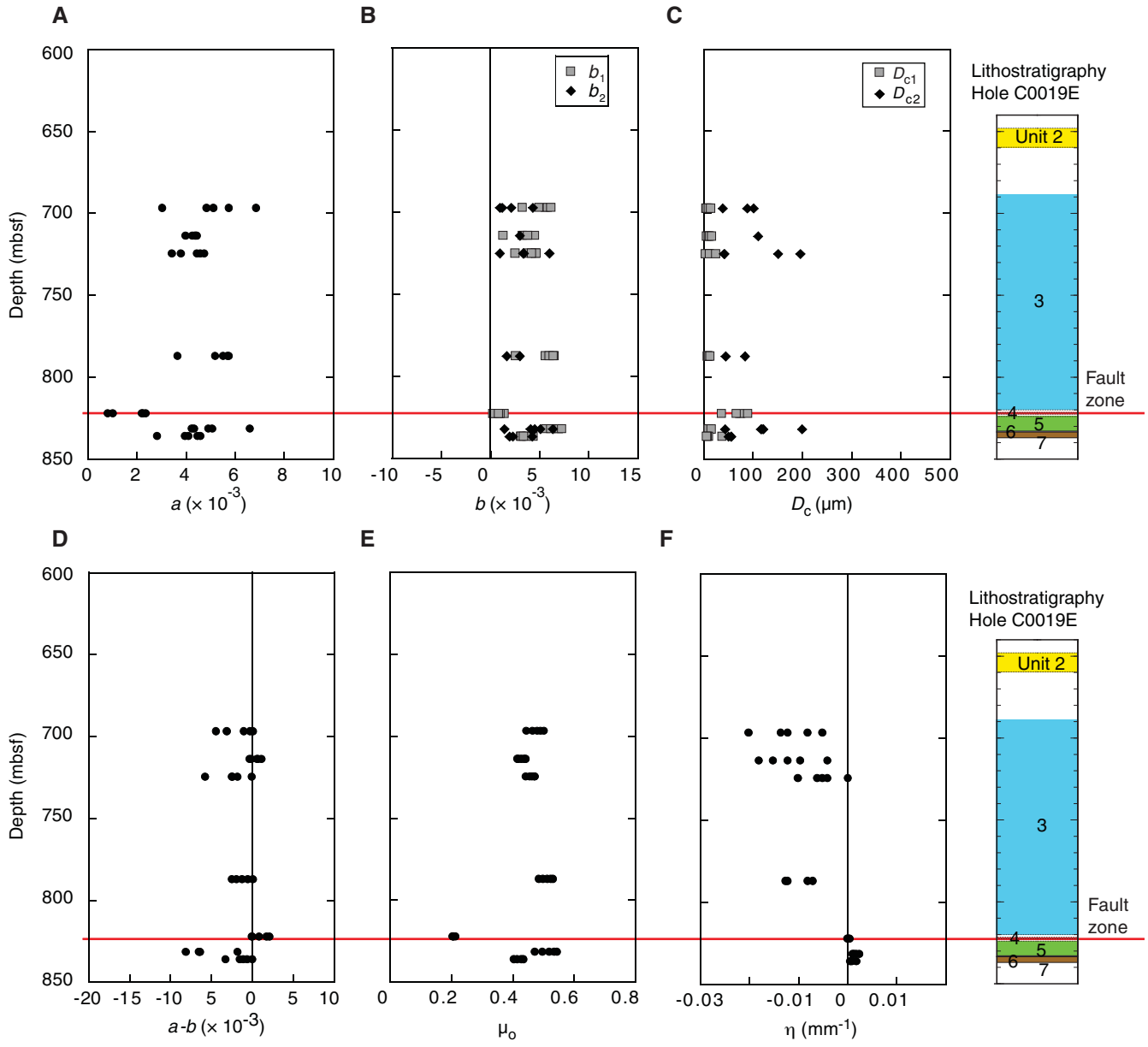

Table T1. Sample and experiment details, Hole C0019E.

Experiment	Sample	Depth	Lithologic unit	Lithology	Testing state	σ_n' during testing (MPa)
	343-C0019E-					
B334	2R-1	648.4	2	Ashy mudstone	Powder	4.9
B358	4R-1	689.4	3	Dark gray siliceous mudstone	Powder	5.4
B351	5R-1	697.2	3	Dark gray siliceous mudstone	Intact	5.5
B337	5R-1	697.2	3	Dark gray siliceous mudstone	Powder	5.5
B318	6R-2	705.9	3	Dark gray siliceous mudstone	Powder	5.6
B356	7R-2	714.4	3	Dark gray siliceous mudstone	Intact	5.7
B365	7R-2	714.4	3	Dark gray siliceous mudstone	Powder	5.7
B320	8R-2	720.4	3	Dark gray siliceous mudstone	Powder	5.8
B357	9R-1	725.0	3	Dark gray siliceous mudstone	Intact	5.9
B366	9R-1	725.0	3	Dark gray siliceous mudstone	Powder	5.9
B328	10R-1	770.2	3	Dark gray siliceous mudstone	Powder	6.5
B321	11R-CC	780.6	3	Dark gray siliceous mudstone	Powder	6.6
B359	12R-2	787.4	3	Dark gray siliceous mudstone	Intact	6.7
B369	12R-2	787.4	3	Dark gray siliceous mudstone	Powder	6.7
B329	13R-2	802.3	3	Dark gray siliceous mudstone	Powder	6.9
B370	14R-2	811.2	3	Dark gray siliceous mudstone	Powder	7.0
B324	16R-1	819.1	3	Dark gray siliceous mudstone	Powder	7.1
B344	17R-1	822.6	4	Sheared scaly clay	Millimeter- to centimeter-scale pieces	7.2
B378	17R-1	822.6	4	Sheared scaly clay	Intact	7.2
B353	17R-1	822.6	4	Sheared scaly clay	Powder	7.2
B325	18R-1	824.9	5	Brown siliceous mudstone	Powder	7.2
B375	18R-1	824.9	5	Brown siliceous mudstone	Powder	7.2
B373	19R-2	828.4	5	Brown siliceous mudstone	Powder	7.3
B350	20R-1	831.9	5	Brown siliceous mudstone	Intact	7.3
B339	20R-1	831.9	5	Brown siliceous mudstone	Powder	7.3
B361	20R-2	833.0	6	Pelagic clay (brown)	Powder	7.3
B352	20R-2	833.1	6	Pelagic clay (pink)	Powder	7.3
B362	20R-2	833.3	6	Pelagic clay (white)	Powder	7.3
B333	21R-1	836.6	2 or 3*	Dark gray siliceous mudstone	Intact	7.4
B343	21R-1	836.6	2 or 3*	Dark gray siliceous mudstone	Powder	7.4

* = interpreted to have originated from a shallower unit.

Table T2. Modeled constitutive friction parameters for powdered samples, Hole C0019E. (Continued on next two pages.)

Experiment	Sample	Depth (mbsf)	v_0 (μm/s)	v (μm/s)	a	b_1	D_{c1}	b_2	D_{c2}	a–b	SD a	SD b_1	SD D_{c1}	SD b_2	SD D_{c2}
	343-C0019E-														
B334	2R-1	648.4	0.1	0.3	0.0055	0.0021	7.8	0.0088	44.3	–0.0054	0.00080	0.00085	8.37	0.00074	3.63
			0.3	1.0	0.0048	0.0047	9.3	0.0089	32.9	–0.0088	0.00072	0.00156	4.84	0.00178	4.37
			1.0	3.0	0.0077	0.0111	13.8	0.0056	91.2	–0.0089	0.00038	0.00041	0.88	0.00032	5.51
			3.0	10.0	0.0085	0.0106	9.1	0.0037	91.2	–0.0058	0.00057	0.00058	0.89	0.00036	11.49
			10.0	30.0	0.0038	0.0060	21.6	0.0145	101.1	–0.0167	0.00034	0.00057	3.20	0.00059	3.50
B358	4R-1	689.4	0.1	0.3	0.0074	0.0086	8.1			–0.0012	0.00056	0.00056	0.69		
			0.3	1.0	0.0074	0.0090	8.0			–0.0016	0.00044	0.00044	0.55		
			1.0	3.0	0.0075	0.0086	6.6	0.0033	136.2	–0.0043	0.00033	0.00032	0.37	0.00010	6.82
			3.0	10.0	0.0057	0.0080	9.0			–0.0023	0.00033	0.00033	0.52		
			10.0	30.0	0.0051	0.0049	9.3	0.0034	134.3	–0.0031	0.00055	0.00052	1.83	0.00021	12.19
B337	5R-1	697.2	0.1	0.3	0.0055	0.0059	9.5	0.0045	36.5	–0.0049	0.00030	0.00063	1.41	0.00069	3.94
			0.3	1.0	0.0067	0.0067	8.1	0.0031	118.0	–0.0032	0.00027	0.00026	0.53	0.00010	6.56
			1.0	3.0	0.0046	0.0052	6.4			–0.0006	0.00067	0.00067	1.37		
			3.0	10.0	0.0076	0.0054	6.5	0.0044	162.3	–0.0023	0.00110	0.00108	1.95	0.00024	14.37
			10.0	30.0	0.0029	0.0035	436.7			–0.0006	0.00010	0.00017	56.03		
B318	6R-2	705.9	0.1	0.3	0.0064	0.0135	5.1	–0.0055	2.8	–0.0016	0.00188	0.00086	0.35	0.00103	2.31
			0.3	1.0	0.0072	0.0103	9.7	0.0036	103.4	–0.0068	0.00026	0.00027	0.47	0.00014	5.35
			1.0	3.0	0.0070	0.0098	10.7			–0.0028	0.00027	0.00027	0.39		
			3.0	10.0	0.0069	0.0082	9.5			–0.0013	0.00032	0.00032	0.53		
			10.0	30.0	0.0049	0.0069	23.8			–0.0020	0.00022	0.00022	1.07		
B365	7R-2	714.4	0.1	0.3	0.0051	0.0047	6.9			0.0004	0.00031	0.00031	0.63		
			0.3	1.0	0.0059	0.0044	4.6	0.0010	51.3	0.0005	0.00034	0.00032	0.56	0.00013	8.47
			1.0	3.0	0.0046	0.0035	4.8	0.0015	53.3	–0.0004	0.00032	0.00031	0.76	0.00014	6.33
			3.0	10.0	0.0052	0.0029	5.8	0.0044	290.3	–0.0021	0.00037	0.00037	1.17	0.00006	11.30
			10.0	30.0	0.0055	0.0035	5.1	0.0035	282.8	–0.0015	0.00072	0.00070	1.29	0.00015	29.60
B320	8R-2	720.4	0.1	0.3	0.0061	0.0067	8.6	0.0017	71.8	–0.0023	0.00022	0.00024	0.60	0.00017	11.21
			0.3	1.0	0.0060	0.0069	9.0	0.0011	211.6	–0.0020	0.00025	0.00025	0.54	0.00014	81.33
			1.0	3.0	0.0041	0.0049	6.4			–0.0008	0.00080	0.00080	2.01		
			3.0	10.0	0.0065	0.0065	7.0	0.0005	66.3	–0.0004	0.00032	0.00033	0.64	0.00020	38.39
			10.0	30.0	0.0050	0.0062	11.2	–0.0030	26.3	0.0017	0.00052	0.00274	4.72	0.00301	16.98
B366	9R-1	725.0	0.1	0.3	0.0041	0.0040	9.0	0.0042	105.7	–0.0041	0.00020	0.00021	0.83	0.00010	3.78
			0.3	1.0	0.0060	0.0054	5.3	0.0063	152.2	–0.0057	0.00028	0.00028	0.44	0.00006	2.86
			1.0	3.0	0.0054	0.0058	8.8	0.0033	179.6	–0.0038	0.00033	0.00032	0.78	0.00009	9.82
			3.0	10.0	0.0046	0.0054	10.7	0.0021	205.0	–0.0029	0.00024	0.00024	0.73	0.00008	14.72
			10.0	30.0	0.0042	0.0030	11.2	0.0036	199.9	–0.0024	0.00032	0.00032	2.05	0.00010	8.49
B328	10R-1	770.2	0.1	0.3	0.0067	0.0057	9.3	0.0030	75.1	–0.0020	0.00033	0.00035	1.09	0.00022	6.77
			0.3	1.0	0.0063	0.0065	8.5	0.0038	66.8	–0.0040	0.00022	0.00021	0.49	0.00014	2.71
			1.0	3.0	0.0061	0.0061	8.0	0.0063	113.1	–0.0064	0.00032	0.00031	0.68	0.00012	3.26
			3.0	10.0	0.0055	0.0070	10.3	0.0029	209.9	–0.0043	0.00017	0.00017	0.45	0.00006	12.40
			10.0	30.0	0.0050	0.0048	10.5			0.0002	0.00083	0.00082	2.70		
B321	11R-CC	780.6	0.1	0.3	0.0073	0.0064	9.0	0.0035	113.8	–0.0027	0.00028	0.00028	0.74	0.00013	6.68
			0.3	1.0	0.0071	0.0088	11.8	0.0021	116.2	–0.0038	0.00023	0.00023	0.50	0.00013	10.60
			1.0	3.0	0.0079	0.0082	8.3	0.0037	85.9	–0.0040	0.00030	0.00029	0.53	0.00014	4.29
			3.0	10.0	0.0072	0.0084	9.3	0.0020	95.3	–0.0032	0.00043	0.00043	0.83	0.00023	13.39
			10.0	30.0	0.0038	0.0057	17.2	0.0062	108.0	–0.0081	0.00038	0.00045	2.40	0.00041	7.07

Table T2 (continued). (Continued on next page).

Experiment	Sample	Depth (mbsf)	v_0 (μm/s)	v (μm/s)	a	b_1	D_{c1}	b_2	D_{c2}	a–b	SD a	SD b_1	SD D_{c1}	SD b_2	SD D_{c2}
	343-C0019E-														
B369	12R-2	787.4	0.1	0.3	0.0058	0.0053	13.8	0.0118	138.4	–0.0113	0.00022	0.00022	1.06	0.00012	2.40
			0.3	1.0	0.0079	0.0087	10.6			–0.0008	0.00023	0.00023	0.36		
			1.0	3.0	0.0063	0.0068	10.0	0.0054	97.6	–0.0059	0.00018	0.00018	0.50	0.00010	2.28
			3.0	10.0	0.0068	0.0079	13.3	0.0021	136.4	–0.0032	0.00016	0.00016	0.46	0.00008	8.76
			10.0	30.0	0.0049	0.0032	11.4	0.0038	56.2	–0.0021	0.00055	0.00063	4.78	0.00064	8.09
B329	13R-2	802.3	0.1	0.3	0.0047	0.0049	6.1			–0.0002	0.00034	0.00034	0.63		
			0.3	1.0	0.0047	0.0053	6.2	0.0017	96.3	–0.0024	0.00034	0.00034	0.67	0.00012	10.22
			1.0	3.0	0.0053	0.0051	4.3	0.0023	164.6	–0.0021	0.00045	0.00004	0.55	0.00007	12.14
			3.0	10.0	0.0042	0.0041	6.7			0.0000	0.00030	0.00030	0.65		
			10.0	30.0	0.0032	0.0014	7.4			0.0019	0.00049	0.00049	4.34		
B370	14R-2	811.2	0.1	0.3	0.0061	0.0069	12.4			–0.0009	0.00025	0.00025	0.67		
			0.3	1.0	0.0066	0.0074	9.9	0.0024	130.0	–0.0032	0.00020	0.00020	0.42	0.00004	9.58
			1.0	3.0	0.0062	0.0082	11.0			–0.0021	0.00019	0.00019	0.36		
			3.0	10.0	0.0057	0.0061	8.8	0.0025	119.5	–0.0029	0.00029	0.00028	0.70	0.00012	7.66
			10.0	30.0	0.0038	0.0046	15.4	0.0034	304.8	–0.0041	0.00023	0.00029	1.79	0.00260	639.46
B324	16R-1	819.1	0.1	0.3	0.0041	0.0058	6.3	0.0037	130.7	–0.0054	0.00038	0.00038	0.71	0.00012	11.27
			0.3	1.0	0.0044	0.0060	8.8	0.0010	140.5	–0.0027	0.00018	0.00018	0.43	0.00007	23.46
			1.0	3.0	0.0048	0.0059	7.7	0.0026	95.0	–0.0037	0.00021	0.00020	0.46	0.00009	4.78
			3.0	10.0	0.0055	0.0061	9.4	0.0025	132.7	–0.0031	0.00026	0.00026	0.57	0.00009	8.23
			10.0	30.0	0.0033	0.0035	16.5			–0.0002	0.00019	0.00019	1.27		
B344	17R-1*	822.6	0.1	0.3	0.0032	0.0019	172.7			0.0013	0.00017	0.00019	55.11		
			0.3	1.0	0.0022	0.0010	80.1			0.0011	0.00023	0.00022	32.32		
			1.0	3.0	0.0018	0.0009	302.8			0.0009	0.00018	0.00042	585.58		
			3.0	10.0	0.0005	0.0008	213.3			–0.0003	0.00020	0.00021	195.52		
B353	17R-1	822.6	0.1	0.3	0.0035	0.0010	37.6			0.0025	0.00030	0.00029	19.27		
			0.3	1.0	0.0041	0.0010	42.8			0.0032	0.00029	0.00028	21.74		
			1.0	3.0	0.0035	0.0008	118.7			0.0027	0.00022	0.00022	77.55		
			3.0	10.0	0.0023	0.0004	140.1			0.0019	0.00024	0.00024	243.13		
			10.0	30.0	0.0020	0.0009	97.4			0.0011	0.00025	0.00024	65.02		
			30.0	100.0	0.0032	0.0009	277.0			0.0023	0.00008	0.00008	81.20		
B375	18R-1	824.9	0.1	0.3	0.0021	0.0010	57.9			0.0011	0.00013	0.00013	17.41		
			0.3	1.0	0.0018	0.0003	39.0			0.0015	0.00019	0.00019	84.37		
			1.0	3.0	0.0001	–0.0007	20.6			0.0008	0.00038	0.00038	20.38		
			3.0	10.0	0.0015	0.0007	95.4			0.0008	0.00009	0.00009	22.20		
			10.0	30.0	0.0051	0.0036	32.8	0.0031	421.6	–0.0016	0.00020	0.00020	3.44	0.00011	54.92
B373	19R-2	828.4	0.1	0.3	0.0063	0.0057	11.0			0.0007	0.00023	0.00023	0.60		
			0.3	1.0	0.0061	0.0060	5.9	0.0043	82.0	–0.0041	0.00029	0.00028	0.44	0.00011	2.64
			1.0	3.0	0.0049	0.0062	6.0	0.0055	84.8	–0.0068	0.00044	0.00044	0.79	0.00018	3.67
			3.0	10.0	0.0055	0.0075	7.4			–0.0020	0.00024	0.00024	0.37		
			10.0	30.0	0.0026	0.0048	15.2			–0.0023	0.00043	0.00043	2.10		
B339	20R-1	831.9	0.1	0.3	0.0063	0.0085	17.5			–0.0022	0.00019	0.00019	0.55		
			0.3	1.0	0.0064	0.0089	12.8			–0.0025	0.00044	0.00044	0.85		
			1.0	3.0	0.0071	0.0079	9.4	0.0108	178.3	–0.0117	0.00025	0.00024	0.46	0.00008	2.85
			3.0	10.0	0.0077	0.0080	8.6	0.0074	91.1	–0.0077	0.00036	0.00036	0.64	0.00018	2.75
			10.0	30.0	0.0072	0.0077	11.2			–0.0006	0.00061	0.00061	1.21		

Table T2 (continued).

Experiment	Sample	Depth (mbsf)	v_0 (μm/s)	v (μm/s)	a	b_1	D_{c1}	b_2	D_{c2}	a–b	SD a	SD b_1	SD D_{c1}	SD b_2	SD D_{c2}
	343-C0019E-														
B361	20R-2 brown	833.0	0.1	0.3	0.0028	0.0017	6.3			0.0011	0.00027	0.00027	1.28		
			0.3	1.0	0.0022	0.0009	4.3			0.0013	0.00034	0.00034	2.47		
			1.0	3.0	0.0019	0.0010	3.5	0.0011	128.3	–0.0001	0.00025	0.00024	1.39	0.00005	14.97
			3.0	10.0	0.0030	0.0022	1.3	0.0006	24.0	0.0002	0.00180	0.00174	1.32	0.00022	11.60
			10.0	30.0	0.0018	0.0015	38.9			0.0003	0.00012	0.00012	4.43		
B352	20R-2 pink	833.1	0.1	0.3	0.0042	0.0024	0.3			0.0019	0.00000	0.00000	0.18		
			0.3	1.0	0.0014	0.0023	224.5			–0.0009	0.00002	0.00003	6.65		
			1.0	3.0	0.0014	0.0003	16.8			0.0011	0.00005	0.00005	5.11		
			3.0	10.0	0.0010	0.0005	303.1			0.0005	0.00004	0.00006	105.26		
			10.0	30.0	0.0010	0.0010	18.8			0.0000	0.00025	0.00025	7.10		
B362	20R-2 white	833.3	0.1	0.3	0.0033	–0.0034	38.5			0.0067	0.00016	0.00016	2.74		
			0.3	1.0	0.0022	–0.0018	16.5			0.0040	0.00018	0.00018	2.24		
			1.0	3.0	0.0022	–0.0016	26.8			0.0038	0.00026	0.00026	6.78		
			3.0	10.0	0.0026	–0.0014	31.8			0.0040	0.00034	0.00034	12.80		
			10.0	30.0	0.0006	–0.0013	42.0			0.0019	0.00059	0.00058	35.64		
B343	21R-1	836.6	0.1	0.3	0.0053	0.0041	11.2	0.0037	69.1	–0.0025	0.00017	0.00022	1.07	0.00018	3.68
			0.3	1.0	0.0051	0.0045	11.9	0.0058	107.6	–0.0051	0.00027	0.00029	1.49	0.00017	5.94
			1.0	3.0	0.0064	0.0057	7.7	0.0055	188.5	–0.0048	0.00022	0.00022	0.43	0.00005	3.54
			3.0	10.0	0.0054	0.0041	8.1	0.0022	87.3	–0.0009	0.00039	0.00039	1.49	0.00019	9.56
			10.0	30.0	0.0041	0.0041	15.3			–0.0001	0.00058	0.00058	3.40		

* = tested as millimeter– to centimeter–scale pieces. SD = standard deviation. See text for parameter definitions.

Table T3. Measured friction parameters for powdered samples, Hole C0019E. (Continued on next page.)

Experiment	Sample	Depth (mbsf)	v_o (μm/s)	v (μm/s)	μ_o	η (mm^{-1})
	343-C0019E-					
B334	2R-1	648.4	0.1	0.3	0.582	0.010
			0.3	1.0	0.569	0.002
			1.0	3.0	0.557	0.002
			3.0	10.0	0.549	–0.010
			10.0	30.0	0.525	–0.010
B358	4R-1	689.4	0.1	0.3	0.563	–0.016
			0.3	1.0	0.549	–0.016
			1.0	3.0	0.535	–0.006
			3.0	10.0	0.523	–0.010
			10.0	30.0	0.512	–0.007
B337	5R-1	697.2	0.1	0.3	0.532	0.006
			0.3	1.0	0.529	–0.010
			1.0	3.0	0.518	–0.005
			3.0	10.0	0.512	–0.025
			10.0	30.0	0.483	–0.014
B318	6R-2	705.9	0.1	0.3	0.520	–0.019
			0.3	1.0	0.500	–0.018
			1.0	3.0	0.477	–0.013
			3.0	10.0	0.460	–0.015
			10.0	30.0	0.443	–0.002
B365	7R-2	714.4	0.1	0.3	0.464	–0.008
			0.3	1.0	0.457	–0.001
			1.0	3.0	0.447	–0.015
			3.0	10.0	0.435	–0.008
			10.0	30.0	0.425	–0.005
B320	8R2-	720.4	0.1	0.3	0.556	–0.010
			0.3	1.0	0.548	–0.019
			1.0	3.0	0.533	–0.022
			3.0	10.0	0.514	–0.013
			10.0	30.0	0.499	–0.013
B366	9R-1	725	0.1	0.3	0.492	–0.011
			0.3	1.0	0.480	–0.007
			1.0	3.0	0.468	–0.005
			3.0	10.0	0.459	–0.008
			10.0	30.0	0.447	–0.008
B328	10R-1	770.2	0.1	0.3	0.515	–0.012
			0.3	1.0	0.505	–0.016
			1.0	3.0	0.489	–0.002
			3.0	10.0	0.480	–0.004
			10.0	30.0	0.471	–0.017
B321	11R-CC	780.6	0.1	0.3	0.498	–0.012
			0.3	1.0	0.488	–0.008
			1.0	3.0	0.477	–0.004
			3.0	10.0	0.468	–0.008
			10.0	30.0	0.456	0.007
B369	12R-2	787.4	0.1	0.3	0.516	–0.001
			0.3	1.0	0.503	–0.012
			1.0	3.0	0.491	–0.008
			3.0	10.0	0.478	–0.003
			10.0	30.0	0.473	0.004
B329	13R-2	802.3	0.1	0.3	0.517	–0.012
			0.3	1.0	0.509	–0.020
			1.0	3.0	0.491	–0.008
			3.0	10.0	0.483	–0.008
			10.0	30.0	0.467	–0.011
B370	14R-2	811.2	0.1	0.3	0.531	–0.014
			0.3	1.0	0.522	–0.014
			1.0	3.0	0.510	–0.010
			3.0	10.0	0.501	–0.003
			10.0	30.0	0.494	–0.003

Table T3 (continued).

Experiment	Sample	Depth (mbsf)	v_o (μm/s)	v (μm/s)	μ_o	η (mm^{-1})
	343-C0019E-					
B324	16R-1	819.1	0.1	0.3	0.484	–0.004
			0.3	1.0	0.477	–0.008
			1.0	3.0	0.468	–0.007
			3.0	10.0	0.459	–0.007
			10.0	30.0	0.450	–0.009
B344	17R-1*	822.6	0.1	0.3	0.213	0.002
			0.3	1.0	0.215	0.002
			1.0	3.0	0.218	0.003
			3.0	10.0	0.221	0.005
B353	17R-1	822.6	0.1	0.3	0.181	0.003
			0.3	1.0	0.183	–0.001
			1.0	3.0	0.186	0.004
			3.0	10.0	0.192	0.004
			10.0	30.0	0.197	0.006
			30.0	100.0	0.201	–0.001
B375	18R-1	824.9	0.1	0.3	0.279	0.002
			0.3	1.0	0.276	–0.001
			1.0	3.0	0.278	0.003
			3.0	10.0	0.280	0.004
			10.0	30.0	0.285	0.002
B373	19R-2	828.4	0.1	0.3	0.495	–0.026
			0.3	1.0	0.483	–0.002
			1.0	3.0	0.476	–0.005
			3.0	10.0	0.462	–0.003
			10.0	30.0	0.457	0.001
B339	20R-1	831.9	0.1	0.3	0.540	–0.024
			0.3	1.0	0.526	–0.024
			1.0	3.0	0.512	–0.005
			3.0	10.0	0.496	0.001
			10.0	30.0	0.484	–0.012
B361	20R-2 brown	833	0.1	0.3	0.295	0.002
			0.3	1.0	0.296	–0.001
			1.0	3.0	0.296	–0.001
			3.0	10.0	0.296	0.004
			10.0	30.0	0.297	0.002
B352	20R-2 pink	833.1	0.1	0.3	0.238	0.004
			0.3	1.0	0.243	0.001
			1.0	3.0	0.243	0.002
			3.0	10.0	0.244	0.002
			10.0	30.0	0.246	0.002
B362	20R-2 white	833.3	0.1	0.3	0.187	0.006
			0.3	1.0	0.196	–0.006
			1.0	3.0	0.195	–0.006
			3.0	10.0	0.197	–0.005
			10.0	30.0	0.200	0.005
B343	21R-1	836.6	0.1	0.3	0.475	0.000
			0.3	1.0	0.469	–0.001
			1.0	3.0	0.459	–0.003
			3.0	10.0	0.451	–0.003
			10.0	30.0	0.444	–0.006

* = tested as millimeter- to centimeter-scale pieces.

Table T4. Modeled constitutive friction parameters for intact samples, Hole C0019E.

Experiment	Sample	Depth (mbsf)	v_o (μm/s)	v (μm/s)	a	b_1	D_{c1}	b_2	D_{c2}	a-b	SD a	SD b_1	SD D_{c1}	SD b_2	SD D_{c2}
	343-C0019E-														
B351	5R-1	697.2	0.1	0.3	0.0069	0.0055	4.8	0.0012	38.4	0.0001	0.00037	0.00038	0.65	0.00026	14.49
			0.3	1.0	0.0058	0.0058	7.8	0.0009	88.1	–0.0010	0.00026	0.00026	0.57	0.00011	21.28
			1.0	3.0	0.0049	0.0049	6.3	0.0043	101.2	–0.0044	0.00029	0.00028	0.65	0.00011	3.57
			3.0	10.0	0.0052	0.0061	9.2	0.0021	843.6	–0.0031	0.00028	0.00027	0.61	0.00051	366.26
			10.0	30.0	0.0031	0.0032	14.4			–0.0002	0.00033	0.00033	2.47		
B356	7R-2	714.4	0.1	0.3	0.0045	0.0032	6.3			0.0012	0.00025	0.00025	0.68		
			0.3	1.0	0.0043	0.0035	5.4			0.0008	0.00038	0.00038	0.78		
			1.0	3.0	0.0044	0.0045	9.4			–0.0001	0.00023	0.00023	0.60		
			3.0	10.0	0.0044	0.0038	11.2			0.0006	0.00022	0.00022	0.89		
			10.0	30.0	0.0040	0.0013	16.2	0.0030	109.6	–0.0003	0.00055	0.00056	19.28	0.00042	15.52
B357	9R-1	725.0	0.1	0.3	0.0046	0.0046	8.0			0.0000	0.00020	0.00020	0.53		
			0.3	1.0	0.0038	0.0046	7.4	0.0010	42.1	–0.0018	0.00034	0.00044	1.35	0.00040	17.40
			1.0	3.0	0.0048	0.0038	4.0	0.0033	40.9	–0.0023	0.00052	0.00052	1.08	0.00028	3.68
			3.0	10.0	0.0045	0.0042	11.5	0.0060	196.0	–0.0057	0.00030	0.00029	1.36	0.00009	5.38
			10.0	30.0	0.0035	0.0025	24.4	0.0033	150.6	–0.0024	0.00024	0.00330	5.85	0.00029	14.11
B359	12R-2	787.4	0.1	0.3	0.0057	0.0056	8.0			0.0001	0.00019	0.00019	0.41		
			0.3	1.0	0.0055	0.0060	7.4			–0.0004	0.00020	0.00020	0.38		
			1.0	3.0	0.0058	0.0065	8.6	0.0017	83.8	–0.0024	0.00015	0.00016	0.35	0.00009	5.05
			3.0	10.0	0.0052	0.0064	10.2			–0.0012	0.00021	0.00021	0.48		
			10.0	30.0	0.0037	0.0026	12.9	0.0030	44.5	–0.0019	0.00034	0.00091	6.64	0.00100	9.71
B378	17R-1	822.6	0.1	0.3	0.0022	0.0004	73.2			0.0018	0.00020	0.00019	91.92		
			0.3	1.0	0.0023	0.0014	75.1			0.0009	0.00017	0.00017	16.56		
			1.0	3.0	0.0024	0.0002	89.4			0.0021	0.00027	0.00027	356.88		
			3.0	10.0	0.0010	0.0010	66.1			0.0000	0.00039	0.00039	53.96		
			10.0	30.0	0.0008	0.0008	35.4			0.0000	0.00048	0.00047	42.46		
B350	20R-1	831.9	0.1	0.3	0.0066	0.0069	10.9	0.0014	117.6	–0.0017	0.00024	0.00024	0.67	0.00012	20.95
			0.3	1.0	0.0043	0.0056	8.7	0.0051	43.5	–0.0064	0.00039	0.00046	1.23	0.00046	3.54
			1.0	3.0	0.0051	0.0069	8.8	0.0045	120.6	–0.0063	0.00045	0.00044	0.94	0.00017	6.63
			3.0	10.0	0.0049	0.0072	9.5	0.0041	116.0	–0.0064	0.00028	0.00028	0.72	0.00014	5.09
			10.0	30.0	0.0044	0.0061	15.1	0.0063	199.2	–0.0081	0.00030	0.00030	1.31	0.00013	6.44
B333	21R-1	836.6	0.1	0.3	0.0045	0.0044	10.2			0.0001	0.00029	0.00029	0.89		
			0.3	1.0	0.0041	0.0031	6.6	0.0042	54.8	–0.0032	0.00037	0.00038	1.51	0.00024	3.37
			1.0	3.0	0.0040	0.0032	6.4	0.0023	50.0	–0.0015	0.00022	0.00022	0.84	0.00015	3.64
			3.0	10.0	0.0046	0.0037	5.5	0.0019	55.1	–0.0011	0.00037	0.00036	0.98	0.00019	6.34
			10.0	30.0	0.0028	0.0034	36.6			–0.0005	0.00038	0.00037	7.24		

SD = standard deviation. See text for parameter definitions.

Table T5. Measured friction parameters for intact samples, Hole C0019E.

Experiment	Sample	Depth (mbsf)	v_o (μm/s)	v (μm/s)	μ_o	η (mm^{-1})
	343-C0019E-					
B351	5R1	697.2	0.1	0.3	0.503	–0.0050
			0.3	1.0	0.492	–0.0120
			1.0	3.0	0.481	–0.0080
			3.0	10.0	0.466	–0.0135
			10.0	30.0	0.447	–0.0200
B356	7R2	714.4	0.1	0.3	0.445	–0.0095
			0.3	1.0	0.439	–0.0120
			1.0	3.0	0.430	–0.0150
			3.0	10.0	0.420	–0.0180
			10.0	30.0	0.417	–0.0040
B357	9R1	725	0.1	0.3	0.474	0.0002
			0.3	1.0	0.472	–0.0040
			1.0	3.0	0.465	–0.0060
			3.0	10.0	0.457	–0.0050
			10.0	30.0	0.444	–0.0100
B359	12R2	787.4	0.1	0.3	0.534	–0.0080
			0.3	1.0	0.526	–0.0125
			1.0	3.0	0.515	–0.0120
			3.0	10.0	0.501	–0.0120
			10.0	30.0	0.488	–0.0070
B375	17R1	822.6	0.1	0.3	0.205	0.0006
			0.3	1.0	0.205	0.0006
			1.0	3.0	0.207	0.0003
			3.0	10.0	0.209	0.0003
			10.0	30.0	0.215	0.0001
B350	20R1	831.9	0.1	0.3	0.547	0.0015
			0.3	1.0	0.537	0.0015
			1.0	3.0	0.521	0.0020
			3.0	10.0	0.498	0.0025
			10.0	30.0	0.474	0.0012
B333	21R1	836.6	0.1	0.3	0.438	0.0020
			0.3	1.0	0.429	0.0020
			1.0	3.0	0.418	0.0020
			3.0	10.0	0.405	0.0007
			10.0	30.0	0.405	0.0010